Tang *et al.*
Chinese Journal of Mechanical Engineering (2022) 35:145
https://doi.org/10.1186/s10033-022-00815-z

Chinese Journal of Mechanical Engineering

ORIGINAL ARTICLE

Open Access

Relative Varying Dynamics Based Whole Cutting Process Optimization for Thin-walled Parts

Yuyang Tang[1], Jun Zhang[1*], Jia Yin[1,2], Lele Bai[1], Huijie Zhang[1] and Wanhua Zhao[1]

Abstract
Thin-walled parts are typically difficult-to-cut components due to the complex dynamics in cutting process. The dynamics is variant for part during machining, but invariant for machine tool. The variation of the relative dynamics results in the difference of cutting stage division and cutting parameter selection. This paper develops a novel method for whole cutting process optimization based on the relative varying dynamic characteristic of machining system. A new strategy to distinguish cutting stages depending on the dominated dynamics during machining process is proposed, and a thickness-dependent model to predict the dynamics of part is developed. Optimal cutting parameters change with stages, which can be divided by the critical thickness of part. Based on the dynamics comparison between machine tool and thickness-varying part, the critical thicknesses are predicted by an iterative algorithm. The proposed method is validated by the machining of three benchmarks. Good agreements have been obtained between prediction and experimental results in terms of stages identification, meanwhile, the optimized parameters perform well during the whole cutting process.

Keywords: Thin-walled parts, Varying dynamics, Frequency response function, Whole cutting process, Optimization

1 Introduction

Thin-walled parts are widely used in airplane for many advantages such as reducing weight, improving space utilization and so on. The thickness of those parts is at least six times lower than the two other relevant directions, thus being flexible and easy to bend [1]. Moreover, large amount of materials (more than 90% of the blank) required to be removed during machining. There is an urgent need to improve efficiency. Those parts are mainly manufactured by high speed milling, where problems can arise related to chatter in the process [2]. The chatter is avoided by predicting stability lobe diagram either in frequency [3, 4] or discrete-time domain [5, 6] based on the structural dynamics of part and machine tool. During machining, the dynamics is variant for part, but invariant for machine tool. Therefore, the relative dynamics varies in cutting process, changing the conditions of stability.

The dynamics of part and machine tool can be obtained by many methods, including experimental modal analysis (EMA), finite element method (FEM), and so on. EMA is a commonly way to measure the dynamics. However, part is physically machined and the process is interrupted for measurements at discrete stations along the toolpath [7, 8], which is prohibitive in production. Meanwhile, the dynamics of machine tool changes with tool and holder, and it is time consuming to be tested by EMA. Therefore, many researchers investigated the methods to predict the dynamics of machine tool and part. Receptance coupling substructure analysis (RCSA) developed by Schmitz et al. [9–12] efficiently predicts the dynamics of the machine tool with different holders and tools. Zhang et al. [13] developed a method to predict the FRFs of tool point with arbitrary spindle orientations based on the frequency

*Correspondence: junzhang@xjtu.edu.cn
[1] State Key Laboratory for Manufacturing Systems Engineering, Xi'an Jiaotong University, Xi'an 710054, China
Full list of author information is available at the end of the article

response function (FRF) measured in three orthogonal postures of the spindle. Besides, Budak et al. [14, 15] also made contribution to improve the RCSA method itself and its accuracy. For the dynamics prediction of part, Meshreki et al. [16] proposed a model based on representing the change of thickness with two-directional multispan plate. Fischer et al. [17] presented a flexible multibody system model for the inside turning of thin-walled cylinders. Ahmadi [18] proposed finite strip modeling for the dynamics prediction of thin-walled parts with complex geometries. Karimi et al. [19] analyzed the dynamics of rectangular plate subjected to a mass moving with variable velocity on a predefined path or an arbitrary one. Wang et al. [20] analyzed the influence factors on natural frequencies of composite materials. In order to improve computational efficiency, Cunedioğlu et al. [21] reduced the order of the FEM by implementing the frequency domain identification methods. Tuysuz and Altintas [22] proposed a frequency-domain model to predict the dynamics of in-process workpiece using reduced order substructuring method, which provides ~ 20 times faster FRF prediction than FEM. Then Tuysuz et al. [23] developed a time-domain model, and the new model is ~ 4 times more computationally efficient than the previous one.

The associated machining optimization based on dynamics have been investigated by many scholars. Altintas et al. [24] analytically predicted the stability lobes in milling based on the dynamics of machine tool. Davies et al. [25] proposed a stability theory for highly interrupted machining, which is always employed in high speed milling. Seguy et al. [26] developed an explicit numerical model to examine the relationship between chatter instability and surface roughness evolution. Kersting et al. [27] predicted regenerative vibrations during the five-axis milling process. Zhou et al. [28] presented an analytical chatter prediction model for bull-nose end milling of aero-engine casings. Liu et al. [29] proposed a prediction method for the stability of free-form surface milling. Shi et al. [30] predicted the thin-walled component milling stability considering material removing process. Bolsunovskly et al. [31] developed a parameters optimization method based on finite element model of part. Yi et al. [32] studied the deformation law and mechanism for milling micro thin wall with mixed boundaries, and obtained the corresponding optimal radial depth of cut and feed per tooth. Ringgaard et al. [33] maximized the material removal rate in milling of thin-walled parts without violating forced vibration and chatter stability. Gu et al. [34] presented three degrees of freedom dynamic model applied to tool chatter for thin-walled structures in milling. Jiang et al. [35] applied reliability analysis of a dynamic structural system to predict chatter of side milling system for machining blisk. Chen et al. [36] obtained force-deformation coupling relationship and time-based deformation matrix of thin-walled milling operation. Sanz-Calle et al. [37] studied the influence of radial engagement and milling direction on stability. For thin-walled part, Yao et al. [38] proposed a position-varying surface roughness prediction method. Ahmed et al. [39] developed a model to determine the part's feasible location for the suitable setup parameters. Guo et al. [40] investigated the effects of feed rate on surface integrity in ultrasonically-assisted vertical milling. Limited researches have been done in the relative varying dynamics based machining. Meshreki et al. [41] mentioned the variation of dominant dynamics from roughing to finishing. Bravo et al. [2] developed a three-dimensional lobe diagram based on the dynamics variation of part to cover the intermediate stages in machining. Tuysuz and Altintas [22] depicted the invariant dynamics of tool and the varying dynamics of part at different stages.

Previous studies mainly focus on partial cutting process. However, the machining efficiency is evaluated for whole cutting process from blank to part, and optimization only for one stage of machining may trap in local optimum. Literatures have not reported the relative varying dynamics based whole cutting process optimization, which is of significance to production.

The paper proposes a novel method of whole cutting process optimization based on the relative varying dynamics of machining system. The strategy of dominated dynamics based cutting stage division and the thickness-dependent dynamics model of part are developed in Section 2. Section 3 presents the multi-variable function of machining efficiency of whole cutting process, and proposes the critical thickness solution method to distinguish stages. The experimental design, results are discussed in Section 4. Section 5 concludes the paper.

2 Relative Varying Dynamics During Thin-walled Part Machining

2.1 Dominated Dynamics Based Cutting Stage Division

Machining system composes of machine tool and part, and its dynamics is influenced by two sub-systems together.

$$[\Delta^m] + [\Delta^p] = [\Delta], \quad (1)$$

where $[\Delta^m]$, $[\Delta^p]$, and $[\Delta]$ represent the dynamics of machine tool, part, and machining system respectively. In three-axis milling with unchangeable tool and its overhang length, $[\Delta^p]$ changes with the material removal in cutting process, while $[\Delta^m]$ keeps constant.

The whole cutting process can be divided into three stages based on the relative dynamics between [Δp] and $[\Delta^m]$. At the beginning (stage 1), as shown in Figure 1(a), the part is thick and can be regarded as rigid. With the material removal, the thickness and stiffness of part decrease, and the dynamics of two subsystems affects the machining process together (stage 2) as depicted in Figure 1(b). At the last stage (stage 3), the dynamics is dominated by part as illustrated in Figure 1(c). The relative dynamic characteristic varies with cutting process for thin-walled parts.

In whole cutting process, the dynamics of machining system is rewritten as a piecewise function based on the thickness of part, expressed as

$$[\Delta]=\begin{cases}[\Delta^m], & t>t_1,\\ [\Delta^m]+[\Delta^p(t)], & t_1\geq t\geq t_2,\\ [\Delta^p(t)], & t_2>t,\end{cases} \tag{2}$$

where t represents the thickness of part; t_1 and t_2 are the critical thicknesses to divide stages; $[\Delta^m]$ can be obtained by the impact testing or RCSA method. However, $[\Delta^p]$ changes with the thickness.

2.2 Modelling of Thickness-dependent Dynamics of Thin-walled Parts

The thickness of part decreases with the material removal. When the dynamics of part influences the machining process, the aspect ratio of the length and height to the thickness is large enough so that the part can be modelled by using Kirchhoff's thin plate theory, in which stress changes in the thickness direction is ignored. The thickness-dependent dynamics model is based on the assumption that the wall of part is reduced from both side simultaneously to remain the neutral plane unchanged during machining. The error of the assumption on the dynamics prediction is negligible [18], and four nodes quadrilateral element is used to mesh the neutral plane.

Based on the vibration of part and the Kirchhoff's thin plate theory, the degree-of-freedom (DOF) of a node in the element can be reduced from 6 to 3, and the shape function of an element can be expressed as

$$\boldsymbol{N}=\begin{bmatrix}N_{n_1} & N_{xn_1} & N_{yn_1} & & & & & & & & & \\ & & & N_{n_2} & N_{xn_2} & N_{yn_2} & & & & & & \\ & & & & & & N_{n_3} & N_{xn_3} & N_{yn_3} & & & \\ & & & & & & & & & N_{n_4} & N_{xn_4} & N_{yn_4}\end{bmatrix}, \tag{3}$$

$$\begin{cases}N_i=\frac{1}{8}\left(1+\frac{x}{x_i}\right)\left(1+\frac{y}{y_i}\right)\left[2+\frac{x}{x_i}\left(1-\frac{x}{x_i}\right)+\frac{y}{y_i}\left(1-\frac{y}{y_i}\right)\right],\\ N_{xi}=-\frac{1}{8}y_r\left(1+\frac{x}{x_i}\right)\left(1+\frac{y}{y_i}\right)^2\left(1-\frac{y}{y_i}\right),\\ N_{yi}=-\frac{1}{8}x_r\left(1+\frac{x}{x_i}\right)^2\left(1+\frac{y}{y_i}\right)\left(1-\frac{x}{x_i}\right),\end{cases}$$
$$(i=n_1,n_2,n_3,n_4), \tag{4}$$

where x_i and y_i (i=n_1, n_2, n_3, n_4) are the coordinates of node in the element coordinate system. $\boldsymbol{B}$ is the independent variable of the stiffness matrix, and is derived from Eqs. (3) and (4):

$$\boldsymbol{B}=\left[\,\boldsymbol{B}_{n_1}\ \boldsymbol{B}_{n_2}\ \boldsymbol{B}_{n_3}\ \boldsymbol{B}_{n_4}\,\right], \tag{5}$$

$$\boldsymbol{B}_r=-\begin{bmatrix}\frac{\partial^2 N_r}{\partial x^2} & \frac{\partial^2 N_{xr}}{\partial x^2} & \frac{\partial^2 N_{yr}}{\partial x^2}\\ \frac{\partial^2 N_r}{\partial y^2} & \frac{\partial^2 N_{xr}}{\partial y^2} & \frac{\partial^2 N_{yr}}{\partial y^2}\\ 2\frac{\partial^2 N_r}{\partial xy} & 2\frac{\partial^2 N_{xr}}{\partial xy} & 2\frac{\partial^2 N_{yr}}{\partial xy}\end{bmatrix},$$
$$(r=n_1,n_2,n_3,n_4). \tag{6}$$

By using the virtual work principle, the stiffness matrix $\boldsymbol{K}^e$ and mass matrix $\boldsymbol{M}^e$ of element are expressed as the function of thickness.

$$\boldsymbol{K}^e(t)=\int_{V^e} t^3\boldsymbol{B}^{\mathrm{T}}\boldsymbol{D}\boldsymbol{B}\mathrm{d}V, \tag{7}$$

where $\boldsymbol{D}$ is the modified bending modulus, and is calculated as

$$\boldsymbol{D}=\frac{E}{12(1-\upsilon^2)}\begin{bmatrix}1 & \upsilon & 0\\ \upsilon & 1 & 0\\ 0 & 0 & (1-\upsilon)/2\end{bmatrix}, \tag{8}$$

where E is the elasticity modulus, and υ is the Poisson ratio of materials.

$$\boldsymbol{M}^e(t)=e_w e_l\rho t\int_{S^e}\boldsymbol{N}^{\mathrm{T}}\boldsymbol{N}\mathrm{d}S, \tag{9}$$

where e_w and e_l are the width and length of element; ρ is the density of material.

The damping matrix can be represented in terms of mass and stiffness matrices. For highly computational efficiency, Rayleigh damping is chosen to establish the damping matrix, which can be formulated as

$$\boldsymbol{C}^e(t)=\alpha\boldsymbol{M}^e(t)+\beta\boldsymbol{K}^e(t), \tag{10}$$

where α and β are damping coefficients identified from experiments.

(See figure on next page.)
Figure 1 Relative varying dynamics in whole cutting process: (**a**) Dynamics dominated by machine tool, (**b**) Dynamics dominated by machine tool and part, (**c**) Dynamics dominated by part

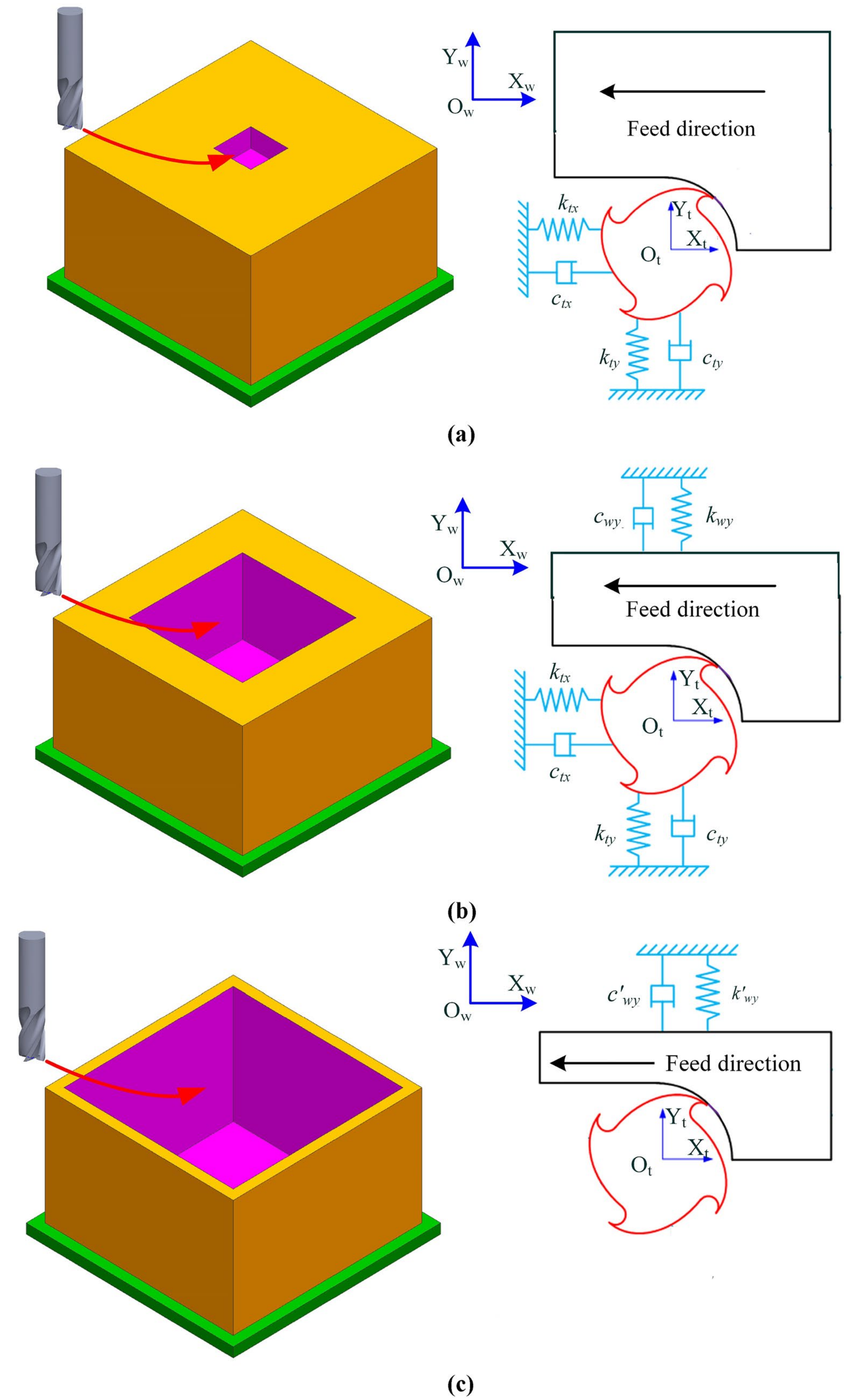

Figure 1 (See legend on previous page.)

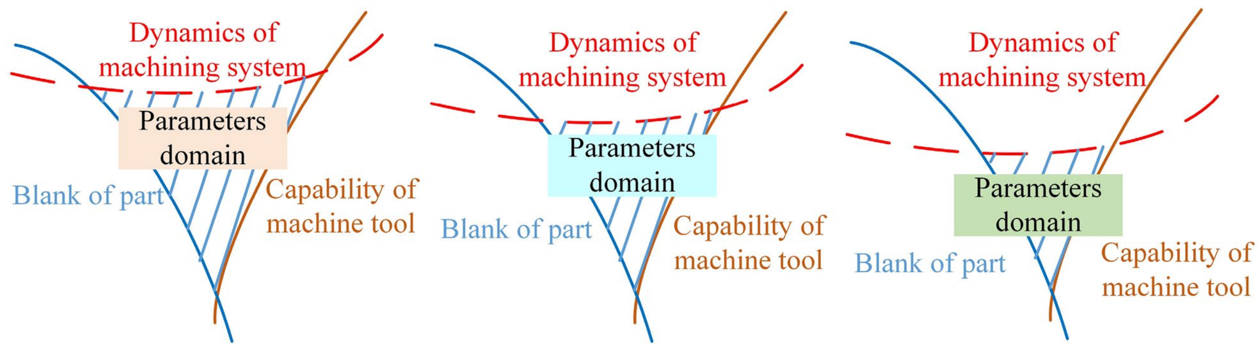

Figure 2 Varying domain of appropriate parameters in whole cutting process

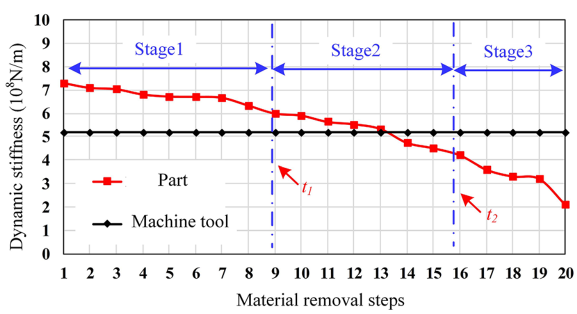

Figure 3 Stage division by critical thickness

To develop the matrices of part, the stiffness matrix, mass matrix and damping matrix of elements need to be assembled in nodes by using matrix displacement method. The dynamics model of the thickness-dependent dynamics of thin-walled part is

$$\boldsymbol{M}(t)\ddot{\boldsymbol{x}} + \boldsymbol{C}(t)\dot{\boldsymbol{x}} + \boldsymbol{K}(t)\boldsymbol{x} = \boldsymbol{F}. \tag{11}$$

$[\Delta^p(t)]$ representing the direct FRFs of the cutting point is solved from the dynamics model, as expressed by

$$[\Delta^p(t)] = \sum_{i=1}^{n} \frac{\boldsymbol{\psi}_{iq}(t)\boldsymbol{\psi}_{iq}^{\mathrm{T}}(t)}{(\omega_i^2(t) - \omega^2) + 2j\zeta_i(t)\omega_i(t)\omega}, \tag{12}$$

where q represents the DOF of lateral deflection in the weakest stiffness point. $\boldsymbol{\Psi}_{iq}$ and ω_i are the eigenvector and eigenvalue of the dynamics model respectively, ζ_i is the modal damping ratio, and n is the number of natural modes considered in synthesizing the FRF.

3 Whole Cutting Process Optimization

3.1 Material Removal Rates of Three Cutting Stages

Cutting conditions including the blank of part, the torque and power capabilities of machine tool, and the dynamics of machining system, determine the selection of cutting parameters. Boundary lines represented those conditions form the parameters domain as shown in Figure 2. The dynamics of machining system varies with stages, leading to the variation of the parameters domain.

The mean material removal rate (*MRR*) is always used to evaluate the machining efficiency, given by

$$MRR(a_e, a_p, f_t, N_t, \Omega) = a_e a_p f_t N_t \Omega, \tag{13}$$

where a_e and a_p are the radial and axial depth of cut. f_t, N_t, and Ω represent the feed per tooth, the number of tooth, and the spindle speed, respectively. The combination of a_p and Ω determines the stability of machining process, which can be expressed as

$$a_p = f_1(k, [\Delta], a_e, N_t^*), \tag{14}$$

$$\Omega = f_2([\Delta], a_p), \tag{15}$$

where k and N_t^* represent the cutting force coefficient and the average number of teeth in the cut, respectively. $[\Delta]$ is expressed as a piecewise function based on the thickness of part. Substituting Eq. (2) into Eq. (13) yields *MRR*, which can be formulated as

$$MRR([\Delta]) = \begin{cases} MRR_1([\Delta^m]), & t > t_1, \\ MRR_2([\Delta^m] + [\Delta^p(t)]), & t_1 \geq t \geq t_2, \\ MRR_3([\Delta^p(t)]), & t_2 > t, \end{cases} \tag{16}$$

where the subscripts (1, 2, 3) of *MRR* represent the cutting stages.

By dividing overall machining into 20 material removal steps with uniform volume, the dynamic stiffness of the part and machine tool are compared as shown in Figure 3. The part's stiffness decreases due to the material removal, but machine tool's stiffness keeps constant during the whole cutting process. The critical thicknesses t_1 and t_2, which are determined based on the stability curve comparison between the machine tool and the part with iterated thickness, divide the whole cutting process into three stages.

The total volume of the removed material can be expressed as

$$v_1(t_{in}, t_1) + v_2(t_1, t_2) + v_3(t_2, t_{fi}) = v, \tag{17}$$

where t_{in} and t_{fi} are the thicknesses of the blank and part, and v is the volume of the material removal, which all can be obtained from the computer aided design (CAD) models. v_1, v_2 and v_3 are the removed volume of each stage, respectively.

The nominal total machining time (T_{ma}) is the sum of stage's, and calculated as

$$\frac{v_1(t_{in}, t_1)}{MRR_1([\Delta^m])} + \frac{v_2(t_1, t_2)}{MRR_2([\Delta^m] + [\Delta^P(t)])} + \frac{v_3(t_2, t_{fi})}{MRR_3([\Delta^P(t)])} = T_{ma}. \tag{18}$$

From Eq. (18), it is easy to conclude that the critical thickness t_1 and t_2 are the key parameters to determine the machining efficiency.

3.2 Critical Thickness Solution Method

The overall solution procedure includes identification module and computational modules as shown in Figure 4. In the identification module, the dimensions of the blank, and the elasticity modulus (E), density (ρ), and Poisson's ratio (v) of the material are recorded. The FRFs of the machine tool (tool point) are tested. The dimensions are used to update the height (h), length (l), and thickness (t) of the chosen plate. E, ρ, and v are used to calculate the dynamics of part.

The computation module for t_1 is divided into four steps. **Step 1**: stability curve of the machine tool is obtained by using its FRFs and stability lobe diagram. The maximum (Max_M) and minimum (Min_M) of the curve is recorded. **Step 2**: The FRF of the part is predicted by substituting the E, ρ, and v, the l, h, and t into the dynamic model developed in Section 2.2. t is divided by a, which is used to update the thickness in each iteration. **Step 3**: stability curve of the part is extracted and minimum (Min_P) is recorded. **Step 4**: h, l, and t are updated until Max_M equals to Min_P. However, it is difficult to obtain this solution exactly. Therefore, the iteration continues until the ratio of the Max_M and Min_P are in [b, d]. The corresponding thickness is the critical thickness t_1. The thickness (t_1) and corresponding length (l'), height (h') are recorded.

In the computational module of t_2, the initial updated parameters are h', l', and t_1, and the process is divided into three steps. **Step 1**: the FRFs of the part is calculated based on the initial parameters, and the thickness is updated by dividing a', which is smaller than a to reduce the updated rate. **Step 2**: stability curve of the part is calculated and maximum (Max_P) is recorded. **Step 3**: if the value of Min_M divided by Max_P is in [b, d], the update of thickness will be terminated and the critical thickness t_2 is obtained.

4 Experimental Verification

4.1 Dynamics Testing of Machine Tool

The testing of dynamics of machine tool is the first step to calculate the critical thicknesses of part. A solid carbide end mill with a diameter of 12 mm and a length of 60 mm was equipped with the machining center DMU50 to machine benchmarks, as shown in Figure 5. The impact hammer (model: PCB 086C03) was used to excite the tool point in the X and Y directions, and the vibration responses were recorded by a low weight accelerometer (model: PCB 352C23). The data was analyzed by the acquisition system (model: Crystal CoCo-80X). The final measured FRFs of tool point was the mean value of the results of 5 times repeated tests. Modal parameters of the machine tool are listed in Table 1.

4.2 Division of Cutting Stages

The machining process of a thin-walled pocket with 1 mm thickness (t), 30 mm height (h) was used to verify the proposed method. The dimensions of blank were 190 mm length (l), 120 mm width (w) as shown in Figure 6, and the material is Al7050 with $E = 71.7$ GPa, $v = 0.33$, $\rho = 2700$ kg/m^3.

Three stages described in Section 2.1 are divided based on the dynamics of part and machine tool. Stability lobe diagrams were calculated by using semi-discretization method [5]. The tangential and radial cutting force coefficients were 8.6×10^8 N/m^2 and 2.47×108 N/m^2 respectively. Down milling was used in machining, and the radial depth of cut was 6 mm, 1.5 mm, and 0.75 mm for stages 1, 2, and 3 respectively.

Table 1 Modal parameters of the machine tool

Direction	Modal mass(kg)	Damp ratio	Modal stiffness (N/m)
X	0.513	0.0139	6.02×10^6
Y	0.572	0.0125	5.4×10^6

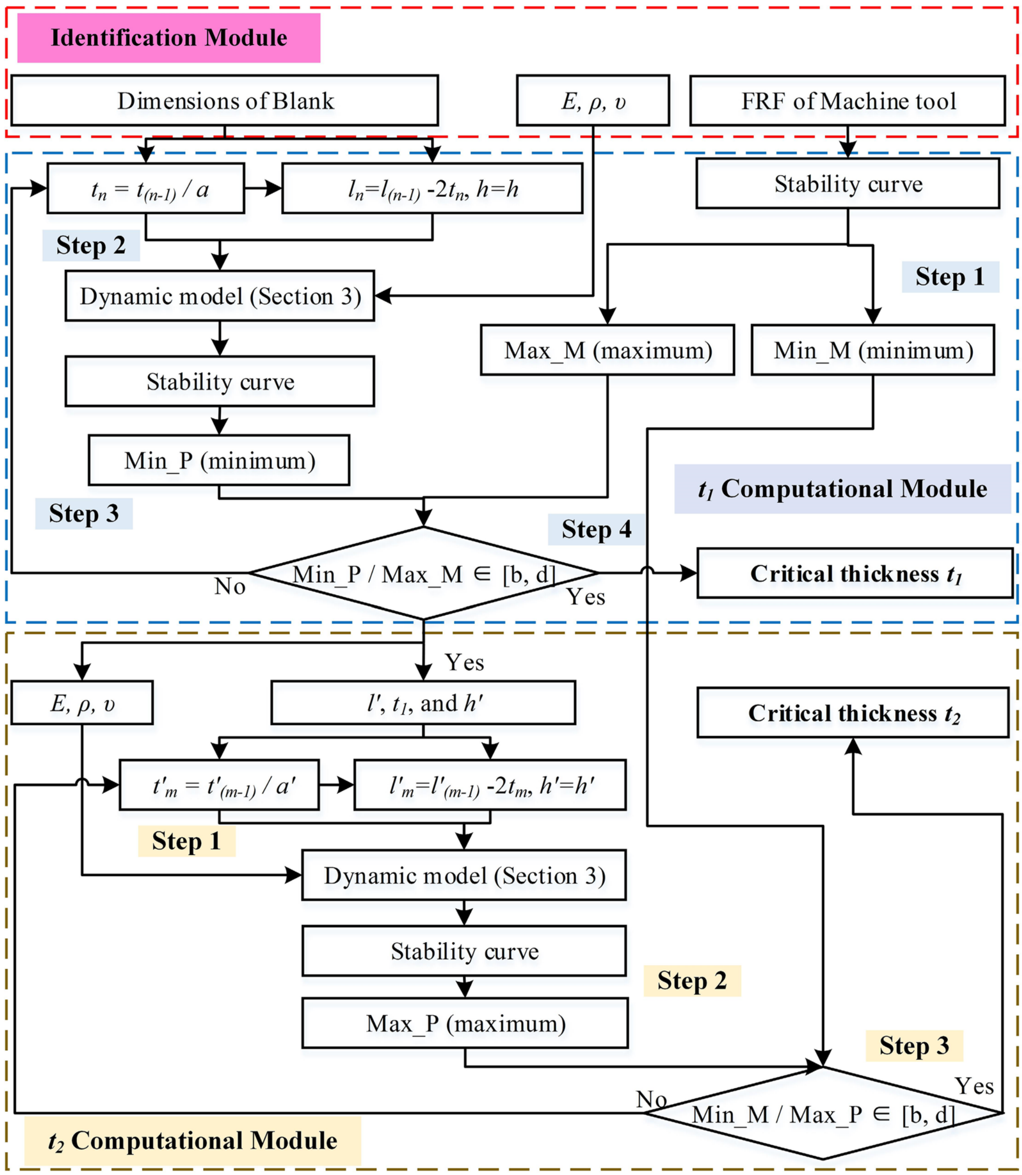

Figure 4 Flowchart of the critical thickness solution method

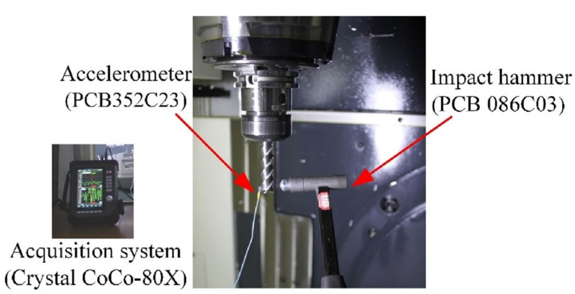

Figure 5 Dynamics testing of machine tool

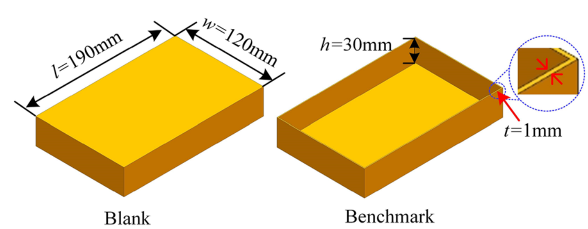

Figure 6 Blank and benchmark

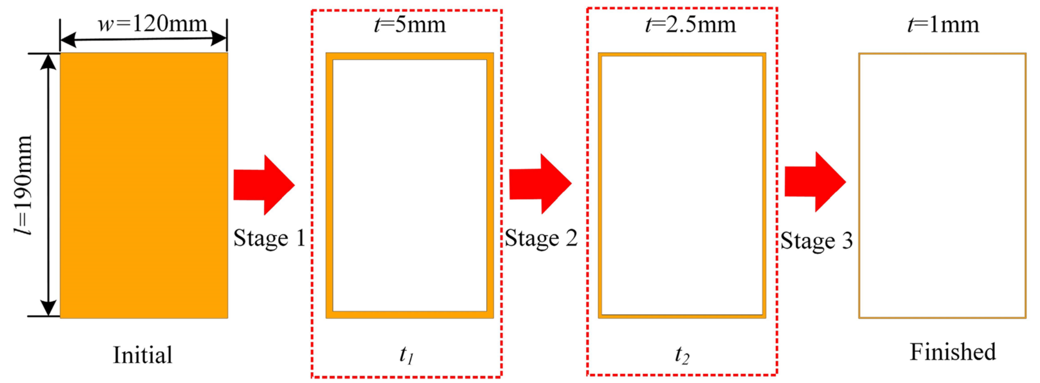

Figure 7 Dimensional changes in three stages

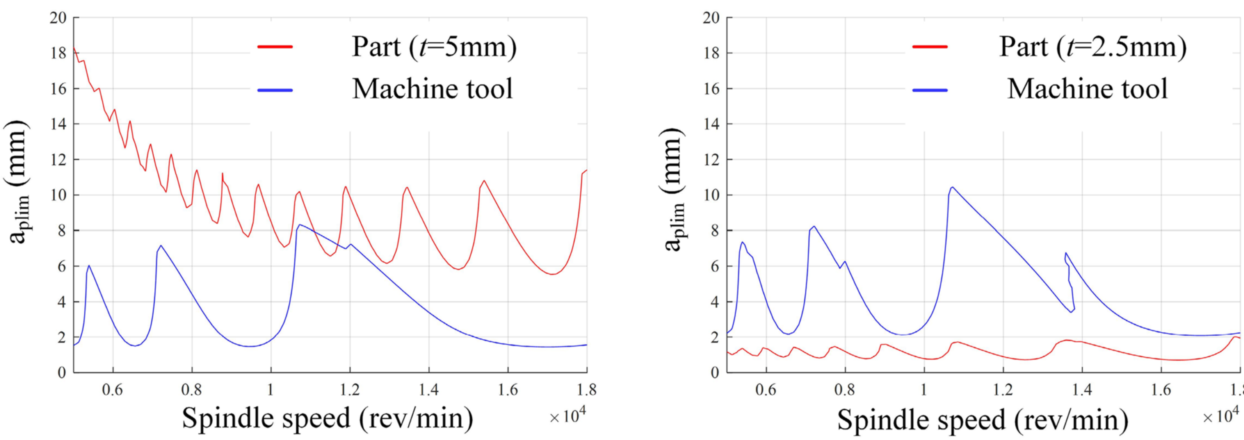

Figure 8 Stability curves of machine tool and part in critical thicknesses

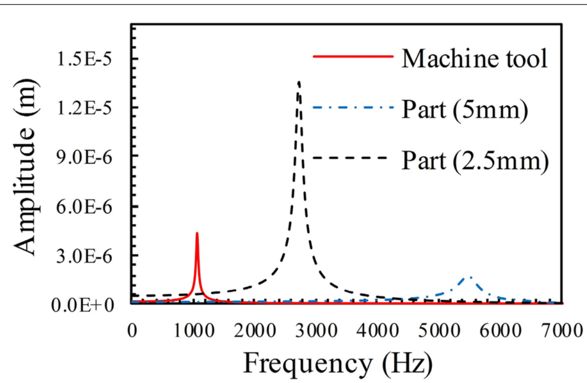

Figure 9 FRFs comparison of machine tool and part in critical thicknesses

The dynamics of machine tool and the dimension and material parameters of part were substituted into the method developed in Section 3.2. a, a', b, and d were set as 2, 1.1, 0.8 and 1.2 respectively. t_1 and t_2 were 5 mm and 2.5 mm by calculation. The corresponding dimensional changes in three stages are illustrated in Figure 7, and the stability curves of machine tool and part in critical thicknesses are shown in Figure 8.

4.3 Selection of Cutting Parameters

FRFs comparisons between the machine tool and the part in two critical thicknesses are shown in Figure 9, which clearly shows that the dominant natural frequencies of the machining system change with the cutting process. At the beginning, the dynamics of the machining system is dominated by the machine tool. When the thickness is between 5 mm and 2.5 mm, the dynamics of the machine tool and part should be both taken into account. In the last stage, the dynamics of the machining process was mainly determined by the part.

Appropriate cutting parameters vary during machining, which should be optimized in each stage based on the dominated dynamics and corresponding stability lobe

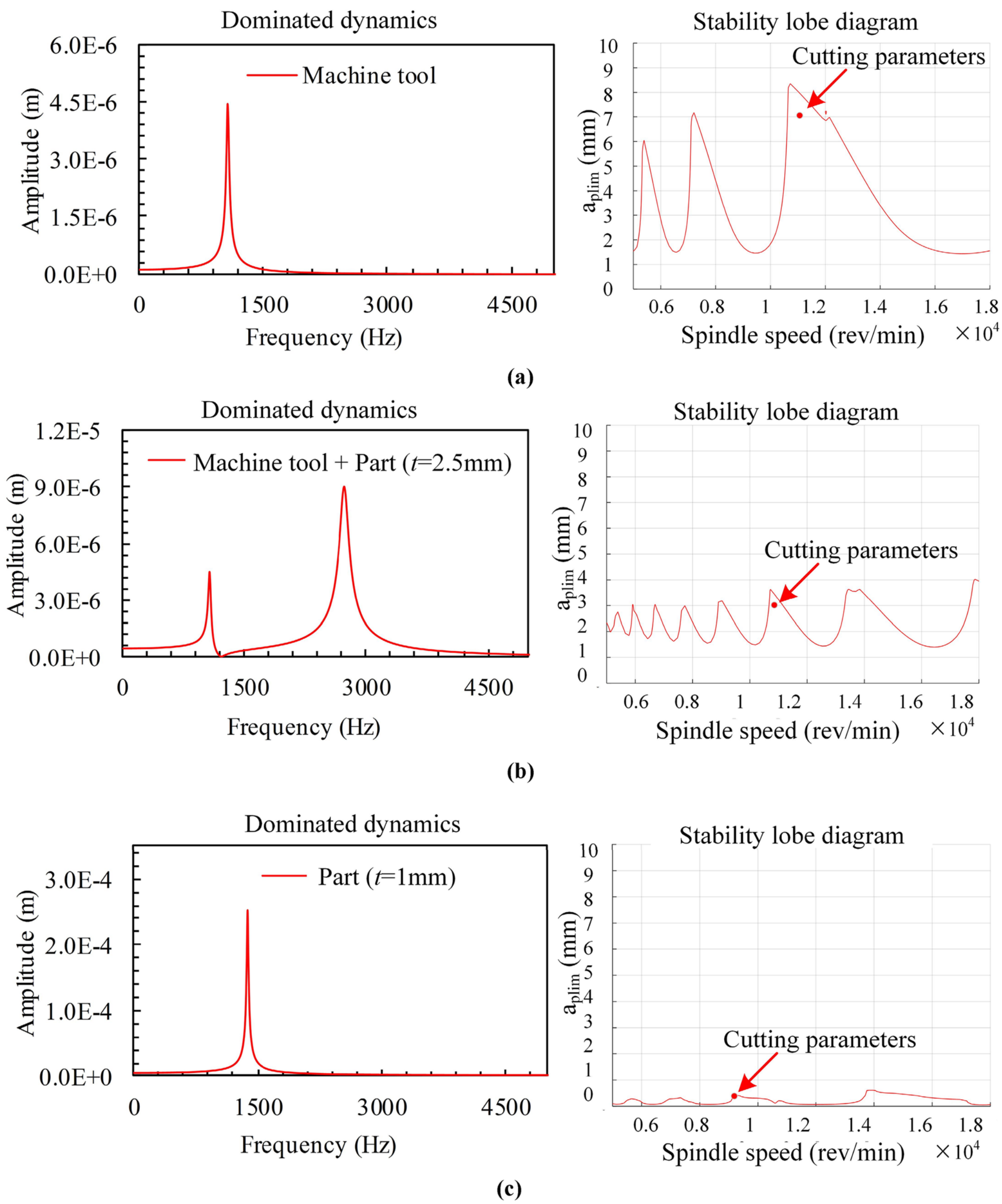

Figure 10 Dominated dynamics and corresponding stability lobe diagrams of three stages: (**a**) Stage 1, (**b**) Stage 1, (**c**) Stage 1

Table 2 Optimized cutting parameters in whole cutting process

Stage	Axial depth (mm)	Radial depth (mm)	Spindle speed (rev/min)	Feed speed (mm/min)
1	7	6	11000	1250
2	3	1.5	11000	1250
3	0.5	0.75	9100	1250

diagram as illustrated in Figure 10. The optimized cutting parameters in whole cutting process are listed in Table 2.

4.4 Experimental Results

Benchmark was machined by the whole cutting process optimization method, and the machining results after three stages are shown in Figure 11. It is clearly seen that

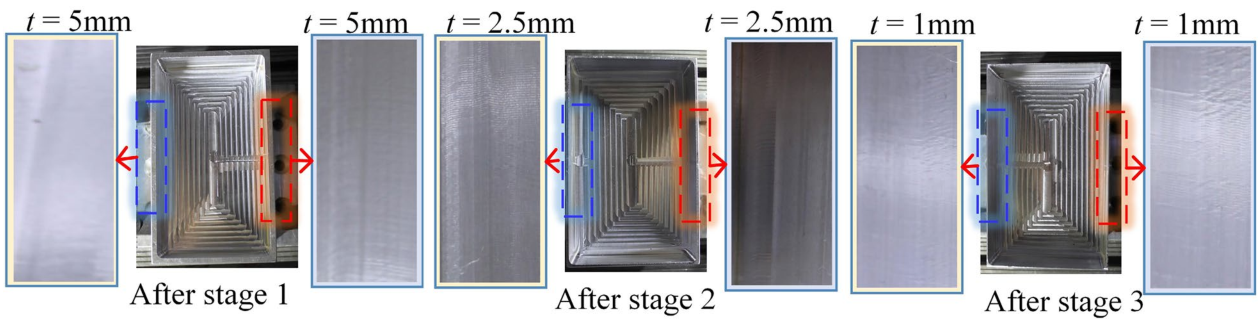

Figure 11 Machining results of Benchmark after three stages

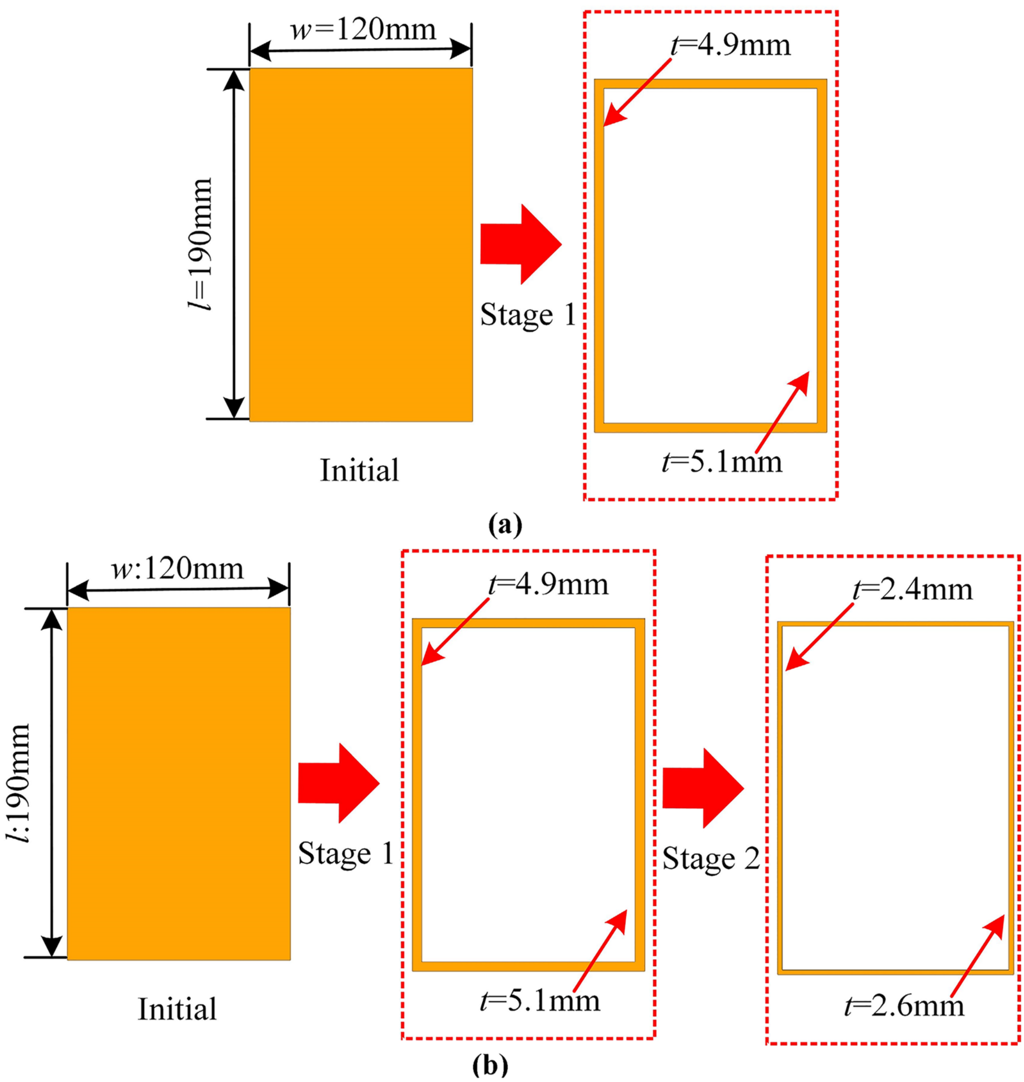

Figure 12 Machining process of: (**a**) Benchmark_1, (**b**) Benchmark_2

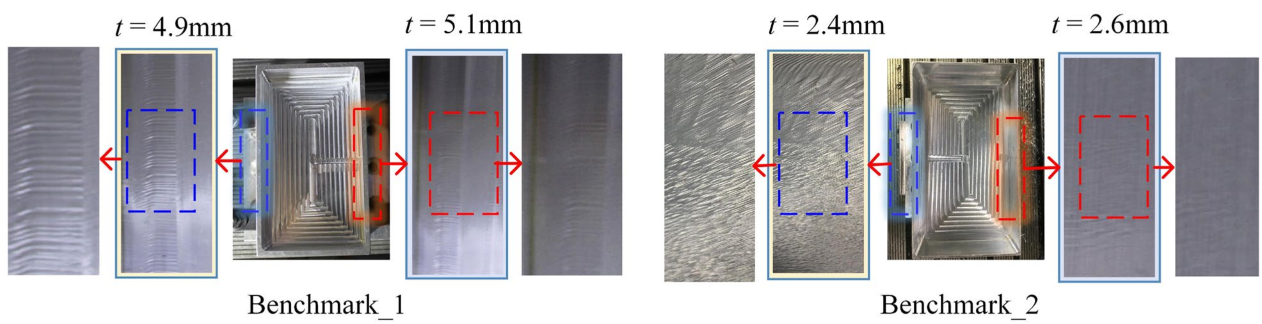

Figure 13 Machining results of benchmark_1 and benchmark_2

the whole cutting process was stable since the cutting parameters are determined by the stability lobe diagrams.

Other two benchmarks (benchmark_1 and benchmark_2) are designed to test the accuracy of critical thickness. At stage 1, the thicknesses of two walls are set to 4.9 mm and 5.1 mm, respectively. At stage 2, they are set to 2.4 mm and 2.6 mm, respectively, as shown in Figure 12. Both the two benchmarks were machined by the cutting parameters of the corresponding stages in Table 2.

The machining results are illustrated in Figure 13. Compared to the previous results in Figure 11, the cutting instability both occurs at t = 4.9 mm and t = 2.4 mm, which indicates the accuracy of the calculated critical thickness.

5 Conclusions

The paper presents a novel method to realize whole cutting process optimization for the thin-walled parts based on relative varying dynamic characteristics of machining system. A number of conclusions can be drawn based on the derivation and validation of the proposed method.

(1) For the thin-walled parts, the whole cutting process is divided into three stages: dynamics dominated by machine tool, both machine tool and part, and part respectively to match the change of stability caused by the relative varying dynamics of machining system.
(2) The cutting parameters are optimized in each stage based on the analysis of stability to make full use of the capabilities of the machining system.
(3) The critical thickness t_1 and t_2 are the key parameters to divide cutting stage and determine the machining efficiency. By using the proposed thickness-dependent dynamics model of part and iterative algorithm, the appropriate critical thicknesses are well predicted.
(4) The method can be used in the whole cutting process optimization of various machining system without going through trial and error based cutting tests.

Nomenclature

a_e: Radial depth of cut; a_p: Axial depth of cut; E: Elasticity modulus of material; f_t: Feed per tooth; k: Cutting force coefficient; MRR: Mean material removal rate; MRR_1: Mean material removal rate of stage1; MRR_2: Mean material removal rate of stage2; MRR_3: Mean material removal rate of stage3; n: Number of natural modes considered in synthesizing the frequency response function; N_t: Number of tooth; N_t^*: Average number of teeth in the cut; q: DOF of lateral deflection in the weakest stiffness point; t: Thickness of part; t_1: Critical thicknesses to divide stage1 and stage2; t_2: Critical thicknesses to divide stage2 and stage3; t_{in}: Thicknesses of blank; t_{fi}: Thicknesses of part; v: Volume of material removal; v_1: Removed volume of stage1; v_2: Removed volume of stage2; v_3: Removed volume of stage3; $\boldsymbol{C}^e$: Damping matrix of element; $\boldsymbol{C}$: Damping matrix of part; $\boldsymbol{K}^e$: Stiffness matrix of element; $\boldsymbol{K}$: Stiffness matrix of part; $\boldsymbol{M}^e$: Mass matrix of element; $\boldsymbol{M}$: Mass matrix of part; α: Damping coefficient of $\boldsymbol{M}^e$; β: Damping coefficient of $\boldsymbol{K}^e$; ζ_i: Modal damping ratio; ρ: Density of material; υ: Poisson ratio of material; $\boldsymbol{\Psi}_{iq}$: Eigenvector of dynamics model; ω_i: Eigenvalue of the dynamics model; Ω: Spindle speed; $[\Delta^m]$: Dynamics of machine tool; $[\Delta^p]$: Dynamics of part; $[\Delta]$: Dynamics of machining system.

Author contributions

YT: methodology, data curation, formal analysis, writing—original draft, review & editing; JZ: conceptualization, supervision, funding acquisition, writing—review and editing; JY: writing—review and editing; LB: validation, writing- review and editing; HZ: formal analysis, validation, writing- review and editing; WZ: conceptualization, supervision, writing—review and editing. All the authors read and approved the final manuscript.

Authors' information

Yuyang Tang, born in 1989, is currently a PhD candidate at *State Key Laboratory for Manufacturing Systems Engineering, Xi'an Jiaotong University, China*. His research interests include cutting dynamics and intelligent machining. E-mail: 642527964@qq.com
Jun Zhang, born in 1978, is currently a professor and a PhD candidate supervisor at *State Key Laboratory for Manufacturing Systems Engineering, Xi'an Jiaotong University, China*. E-mail: junzhang@xjtu.edu.cn
Jia Yin, born in 1981, is currently a PhD candidate at *State Key Laboratory for Manufacturing Systems Engineering, Xi'an Jiaotong University*, and a senior engineer at *AVIC Xi'an Aircraft Industry Group Company Ltd., China*. E-mail: yinjia6@163.com
Lele Bai, born in 1994, is currently a PhD candidate at *State Key Laboratory for Manufacturing Systems Engineering, Xi'an Jiaotong University, China*. E-mail: lelebai@stu.xjtu.edu.cn

Huijie Zhang, born in 1983, is currently an engineer at *State Key Laboratory for Manufacturing Systems Engineering, Xi'an Jiaotong University, China*. E-mail: zhj3632@163.com
Wanhua Zhao, born in 1965, is currently a professor and a PhD candidate supervisor at *State Key Laboratory for Manufacturing Systems Engineering, Xi'an Jiaotong University, China*. E-mail: whzhao@xjtu.edu.cn

Funding
Supported by National Key R&D Program of China (Grant No. 2018YFB1701901), and Guangdong Provincial Key-Area Research and Development Program (Grant No. 2020B090927002).

Availability of data and materials
The datasets supporting the conclusions of this article are included within the article.

Consent for publication
Not applicable.

Competing interests
The authors declare no competing financial interests.

Author Details
[1]State Key Laboratory for Manufacturing Systems Engineering, Xi'an Jiaotong University, Xi'an 710054, China. [2]AVIC Xi'an Aircraft Industry Group Company Ltd, Xi'an 710089, China.

Received: 31 December 2021 Revised: 28 July 2022 Accepted: 7 November 2022
Published online: 03 December 2022

References

[1] S I Del, A Rivero, L L N de López, et al. Thin-wall machining of light alloys: A review of models and industrial approaches. *Materials,* 2019, 12(12): 2012.
[2] U Bravo, O Altuzarra, L L N de López, et al. Stability limits of milling considering the flexibility of the workpiece and the machine. *International Journal of Machine Tools and Manufacture,* 2005, 45(15): 1669–1680.
[3] J Tlusty, W Zaton, F Ismail. Stability lobes in milling. *CIRP Annals,* 1983, 32(1): 309–313.
[4] Y Altintaş, E Budak. Analytical prediction of stability lobes in milling. *CIRP Annals,* 1995, 44(1): 357–362.
[5] T Insperger, G Stépán. Updated semi-discretization method for periodic delay-differential equations with discrete delay. *International Journal for Numerical Methods in Engineering,* 2010, 61(1): 117–141.
[6] Y Ding, L M Zhu, X J Zhang, et al. A full-discretization method for prediction of milling stability. *International Journal of Machine Tools and Manufacture,* 2010, 50(5): 502–509.
[7] J H Li, Z Kilic. Murat, Y Altintas. General cutting dynamics model for five-axis ball-end milling operations. *Journal of Manufacturing Science and Engineering,* 2020, 142(12): 121003.
[8] F Ismail, R Ziaei. Chatter suppression in five-axis machining of flexible parts. *International Journal of Machine Tools and Manufacture,* 2002, 42(1): 115–122.
[9] T L Schmitz, R R Donalson. Predicting high-speed machining dynamics by substructure analysis. *CIRP Annals,* 2000, 49(1): 303–308.
[10] T L Schmitz, M A Davies, M D Kennedy. Tool point frequency response prediction for high-speed machining by RCSA. *Journal of Manufacturing Science and Engineering,* 2001, 123(4): 700–707.
[11] T L Schmitz, M A Davies, K Medicus, et al. Improving high-speed machining material removal rates by rapid dynamic analysis. *CIRP Annals,* 2001, 50(1): 263–268.
[12] T L Schmitz, K Powell, D Won, et al. Shrink fit tool holder connection stiffness/damping modeling for frequency response prediction in milling. *International Journal of Machine Tools and Manufacture,* 2007, 47(9): 1368–1380.
[13] J Zhang, J H Li, Z N Xie, et al. Rapid dynamics prediction of tool point for bi-rotary head five-axis machine tool. *Precision Engineering,* 2017, 48: 203–215.
[14] E Budak, A Ertürk, H N Özgüven. A modeling approach for analysis and improvement of spindle-holder-tool assembly dynamics. *CIRP Annals,* 2006, 55(1): 369–372.
[15] M Namazi, Y Altintas, T Abe, et al. Modeling and identification of tool holder–spindle interface dynamics. *International Journal of Machine Tools and Manufacture,* 2007, 47(9): 1333–1341.
[16] M Meshreki, H Attia, J Kövecses. Development of a new model for the varying dynamics of flexible pocket-structures during machining. *Journal of Manufacturing Science and Engineering,* 2011, 133(4): 041002.
[17] A Fischer, P Eberhard, J Ambrósio. Parametric flexible multibody model for material removal during turning. *Journal of Computational and Nonlinear Dynamics,* 2014, 9(1): 011007.
[18] K Ahmadi. Finite strip modeling of the varying dynamics of thin-walled pocket structures during machining. *Int. J. Adv. Manuf. Technol.,* 2017, 89(9–12): 2691–2699.
[19] A H Karimi, S Alahdadi, M Ghayour. Dynamic analysis of a rectangular plate subjected to a mass moving with variable velocity on a predefined path or an arbitrary one. *Thin-Walled Structures,* 2021, 160: 107340.
[20] B Wang, F Zhao, Z X Zhao, et al. Influence factors on natural frequencies of composite materials. *Frontiers of Mechanical Engineering,* 2020, 15(4): 571–584.
[21] Y Cunedioğlu, A Muğan, H Akçay. Frequency domain analysis of model order reduction techniques. *Finite Elements in Analysis and Design,* 2006, 42(5): 367–403.
[22] O Tuysuz, Y Altintas. Frequency domain updating of thin-walled workpiece dynamics using reduced order substructuring method in machining. *Journal of Manufacturing Science and Engineering,* 2017, 139(7): 071013.
[23] O Tuysuz, Y Altintas. Time-domain modeling of varying dynamic characteristics in thin-wall machining using perturbation and reduced-order substructuring methods. *Journal of Manufacturing Science and Engineering,* 2018, 140(1): 011015.
[24] Y Altıntas, E Shamoto, P Lee, et al. Analytical prediction of stability lobes in ball end milling. *Journal of Manufacturing Science and Engineering,* 1999, 121(4): 586–592.
[25] M A Davies, J R Pratt, B S Dutterer, et al. The stability of low radial immersion milling. *CIRP Annals,* 2000, 49(1): 37–40.
[26] S Seguy, G Dessein, L Arnaud. Surface roughness variation of thin wall milling, related to modal interactions. *International Journal of Machine Tools and Manufacture,* 2008, 48(3–4): 261–274.
[27] P Kersting, D Biermann. Simulation concept for predicting workpiece vibrations in five-axis milling. *Machining Science and Technology,* 2009, 13(2): 196–209.
[28] X Zhou, D H Zhang, M Luo, et al. Chatter stability prediction in four-axis milling of aero-engine casings with bull-nose end mill. *Chinese Journal of Aeronautics,* 2015, 28(6): 1766–1773.
[29] X L Liu, R V Li, S Wu, et al. A prediction method of milling chatter stability for complex surface mold. *Int. J. Adv. Manuf. Technol.*, 2017; 89(9–12): 2637–2648.
[30] J H Shi, Q H Song, Z Q Liu, et al. A novel stability prediction approach for thin-walled component milling considering material removing process. *Chinese Journal of Aeronautics,* 2017, 30(5): 1789–1798.
[31] S Bolsunovskiy, V Vermel, G Gubanov, et al. Thin-walled part machining process parameters optimization based on finite-element modeling of workpiece vibrations. *Procedia CIRP,* 2013, 8: 276–280.
[32] J Yi, X B Wang, L Jiao, et al. Research on deformation law and mechanism for milling micro thin wall with mixed boundaries of titanium alloy in mesoscale. *Thin-Walled Structures,* 2019, 144: 106329.
[33] K Ringgaard, Y Mohammadi, C Merrild, et al. Optimization of material removal rate in milling of thin-walled structures using penalty cost function. *International Journal of Machine Tools and Manufacture,* 2019, 145: 103430.
[34] D Gu, Y Wei, B Xiong, et al. Three degrees of freedom chatter stability prediction in the milling process. *Journal of Mechanical Science and Technology,* 2020, 34(9): 3489–3496.

[35] G J Jiang, D W Wu, N Zhang, et al. Chatter reliability prediction of side milling aero-engine blisk. *Journal of Mechanical Science and Technology,* 2020, 34: 1–9.
[36] Z T Chen, C X Yue, S Y Liang, et al. Iterative from error prediction for side-milling of thin-walled parts. *The International Journal of Advanced Manufacturing Technology,* 2020, 107(9): 4173–4189.
[37] M Sanz-Calle, J Munoa, A Iglesias, et al. The influence of radial engagement and milling direction for thin wall machining: a semi-analytical study. *Procedia CIRP,* 2021, 102: 180–185.
[38] Z Q Yao, C Fan, Z Zhang, et al. Position-varying surface roughness prediction method considering compensated acceleration in milling of thin-walled workpiece. *Frontiers of Mechanical Engineering,* 2021, 16: 855–867.
[39] A Ahmed, M Wasif, A Fatima, et al. Determination of the feasible setup parameters of a workpiece to maximize the utilization of a five-axis milling machine. *Frontiers of Mechanical Engineering,* 2021, 16(2): 298–314.
[40] S Guo, W Du, Q H Jiang, et al. Surface integrity of ultrasonically-assisted milled Ti6Al4V alloy manufactured by selective laser melting. *Chin. J. Mech. Eng.,* 2021, 34(1): 67.
[41] M Meshreki, H Attia, J Kövecses. A new analytical formulation for the dynamics of multipocket thin-walled structures considering the fixture constraints. *Journal of Manufacturing Science and Engineering,* 2011, 133(2): 021014.